

Available online at www.sciencedirect.com

ScienceDirect

journal homepage: www.elsevier.com/locate/ijhydene

Performance improvement of a photovoltaic system using a controller redesign based on numerical modeling

Onur Deveci*, Coşku Kasnakoğlu

TOBB University of Economics and Technology, Department of Electrical and Electronics Engineering, 06560, Ankara, Turkey

ARTICLE INFO

Article history:

Received 24 November 2015

Received in revised form

13 May 2016

Accepted 17 May 2016

Available online 13 June 2016

Keywords:

Solar energy

Photovoltaics

Voltage regulation

MPPT

Simulation

MATLAB

ABSTRACT

This paper focuses on the utilization of numerical modeling and simulation to improve the performance of a theoretically designed stand-alone photovoltaic (PV) system with constant DC voltage. A theoretically designed system based on standard methods found in the literature is modeled and simulated numerically. This system reveals some unexpected behavior when it is subjected to certain irradiation, temperature and load changes. This behavior is due to the parameters and dynamics of real circuit elements not taken into account by the design. It is also problematic that one cannot use conventional linearization methods to model the system and design the controller because the system contains large nonlinearities caused by elements such as DC/DC switching converters driven by pulse width modulation (PWM). This requires the use of an alternate technique based on the use of simulated input/output data to determine an operating point around which a linear system model is derivable. The controllers for the PV system are redesigned using these models, and the closed-loop system is simulated with variable temperature, irradiation and load levels. Upon evaluating the system performance reveals that the redesigned control system is capable of operating the PV panel at its maximum power point under different atmospheric and load conditions and can provide a constant DC voltage to the critical load while charging the battery with the extra power from the panel.

© 2016 Hydrogen Energy Publications LLC. Published by Elsevier Ltd. All rights reserved.

Introduction

Traditional energy resources are expected to deplete in the near future and cannot support an increasing population and increasing industrialization. The gap between production and energy consumption is increasing continuously [1]. Additional

environmental issues arising from the production and consumption of traditional energy resources have increased the interest in renewable energy sources worldwide.

Solar energy is one of the most popular renewable energy sources due to its low operational cost, long lifecycle and unlimited supply. There are many additional advantages of solar energy utilization: there are no moving parts, no fuels

* Corresponding author. Tel.: +90 312 292 4061; fax: +90 312 292 4091.

E-mail address: odeveci@etu.edu.tr (O. Deveci).

<http://dx.doi.org/10.1016/j.ijhydene.2016.05.149>

0360-3199/© 2016 Hydrogen Energy Publications LLC. Published by Elsevier Ltd. All rights reserved.

emitted during operation, it is suitable for stand-alone operation, installation is easy, a system can withstand severe weather conditions and maintenance is infrequent [2]. Moreover, the environmental impact of solar energy is less than that of traditional energy sources, and solar energy technology is constantly improving [3]. In the current literature, there is much research on solar energy systems, including solar water pumping systems [4], power electronic interfaces [5] and grid-connected PV systems [6]. These PV research and development activities have increased the demand for solar energy, with an average increase of 20–25% each year in the last 20 years [7,8]. The most important factors contributing to the increase in demand are production technology improvements which have resulted in reduced production costs and an increase in solar cell efficiency.

Load profile and atmospheric conditions affect the amount of solar power obtained from PV panels [9,10]. An increase in solar radiation increases the output current of the panel whereas an increase of the outside temperature decreases the voltage at the panel terminals. Consequently, the maximum power that can be obtained from the PV panel depends on the atmospheric conditions. In the literature, several maximum power point tracking (MPPT) methods can be found that, depending on load profile and atmospheric conditions, can be used to operate a PV panel at its maximum power point [10–15]. Among these, Perturb & Observe (P&O) and Incremental Conductance (IC) are the most commonly used algorithms. Through the use of maximum power point tracking algorithms, higher power output can be achieved with fewer PV panels and lower cost PV systems [16]. Other than MPPT, inverters (for grid-connected or stand-alone AC systems), DC/DC converters (buck, boost, buck-boost, Cúk, SEPIC etc.) and electric batteries (lead acid/lithium-ion) can be used to improve panel efficiency and output voltage regulation [17].

Several works in the literature can be found regarding the design of stand-alone PV systems including research on hybrid systems [18–25], approaches to alternative controller designs [26–28] and improvement strategies based on system reconfiguration and optimization [29,30]. These studies commonly employ empirical approaches to controller design or use standardized models for the converters that represent the system behavior between given input/output ports. It is however possible that these standard models are invalid when the system topology and operating conditions are changed. Repeating analytical derivations for every such change is cumbersome and time consuming. Some configurations can also be numerically ill-conditioned, leading to the typical linearization methods to fail. Moreover, in a complex system with many controllers, the modelling and design procedure needs to be repeated from the input/output perspective of each controller. Therefore a numerical approach capable of producing mathematical models of the system between any given input/output points and control design based on these models would be greatly beneficial.

In this study, a commonly used PV system configuration (e.g. Ref. [31]) is taken as a case study to introduce a data based modelling and control design approach capable of addressing the points mentioned above. Accurate numerical

models are used to observe the effects of realistic PV panel models, DC/DC converters, battery types and controller type, as well as different irradiation, temperature and load conditions. The main challenge regarding controller design for these systems is outlined. For a non-empirical systematic controller design, one needs to obtain a mathematical model describing the process, but standard linearization methods fail to produce such a model because of switching effects and nonlinearities. This is overcome by using simulated input/output data to generate a point for desired operation around which a linear model is obtained and used in controller design to improve the performance of the original empirically designed controllers. A comparison of the systems through numerical simulations shows notable improvements in output voltage regulation and battery charging performance under varying atmospheric and load characteristics.

Modeling and control design

For numerical modeling and simulations and to develop control systems and test system-level performance, we use the MATLAB numerical computing environment together with its graphical programming environment, Simulink, along with its various toolboxes, which provide component libraries and analysis tools for modeling and simulating electrical power systems. Each sub-system incorporating PV panels, DC/DC converters, electric battery and load is modeled and simulated as detailed in Section [Numerical Realization in MATLAB/Simulink](#). PV cell equivalent circuit equations is utilized to model the PV panel, bidirectional DC/DC converter (BDC) and unidirectional DC/DC converter (UDC) linearized average state-space equations were used to model the converter and design the controller, and a standard built-in battery model is used to model lead acid batteries.

System configuration

System configuration is based on a commonly used arrangement in the literature [31], whose overall structure is given in [Fig. 1](#). A unidirectional boost converter between the solar panels and load is used for MPPT control, and a bidirectional boost converter between the battery and the load is used for battery charging/discharging control.

The power flow within the system is categorized during normal operation, PV/SOC regulation and PV/DC-link regulation. For each regulation scenario, a control structure is designed as given in [Fig. 2](#). During normal operation, v_{pv-ref} is generated solely by the MPPT module, and the other two loops, PI_1 and PI_2 , remained idle. The unidirectional converter ensures maximum power is delivered to the load and the bidirectional converter provides the power balance. During PV/SOC regulation, the PI_1 loop ensures that the battery is not charged beyond a maximum charge level by disturbing the MPPT reference voltage. During PV/DC-link regulation, the PI_2 loop ensures that the DC-link voltage is not increased beyond a predefined limit also by disturbing the MPPT reference voltage.

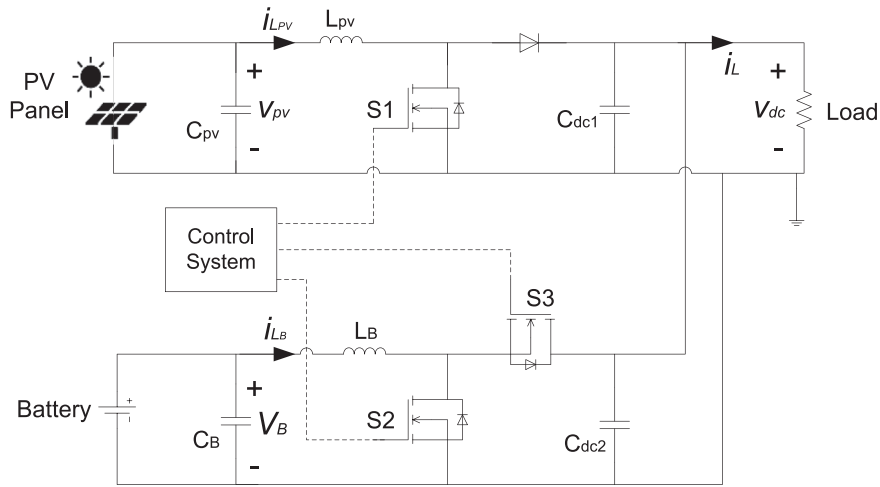


Fig. 1 – PV system configuration. [31].

Mathematical model

The linearized average state-space equations for the unidirectional converter are given in Eqs. (1) and (2) and the linearized average state space equations for the bidirectional boost converter are given in Eq. (3) and (4).

$$L_{pv} \frac{di_{L_{pv}}}{dt} = v_{pv} + V_{dc}d \tag{1}$$

$$C_{pv} \frac{dv_{pv}}{dt} = -i_{L_{pv}} + \frac{v_{pv}}{r_{pv}} \tag{2}$$

$$L_B \frac{di_{L_B}}{dt} = -(1-D)v_{dc} + V_{dc}d \tag{3}$$

$$C \frac{dv_{dc}}{dt} = (1-D)i_{L_B} - \frac{v_{dc}}{R} - V_{dc}d \tag{4}$$

where L_{pv} is the inductor of the unidirectional converter, $i_{L_{pv}}$ is the input current of the unidirectional converter, v_{pv} is the PV panel terminal voltage, V_{dc} is the nominal DC-link voltage across the load, r_{pv} is the dynamic resistance of the PV array around the operating point, d is the averaged control input, L_B is the inductor of the bidirectional converter, i_{L_B} is the inductor current of the bidirectional converter, D is the duty cycle, C is the combination of $C_{dc1} + C_{dc2}$ and R is the load resistance. Transfer functions for the PI controllers are selected empirically, as described in Ref. [31] and as given in Eq. (5) to Eq. (10)

$$G_{PI-pv1} = 0.5 + 250 \frac{1}{s} \tag{5}$$

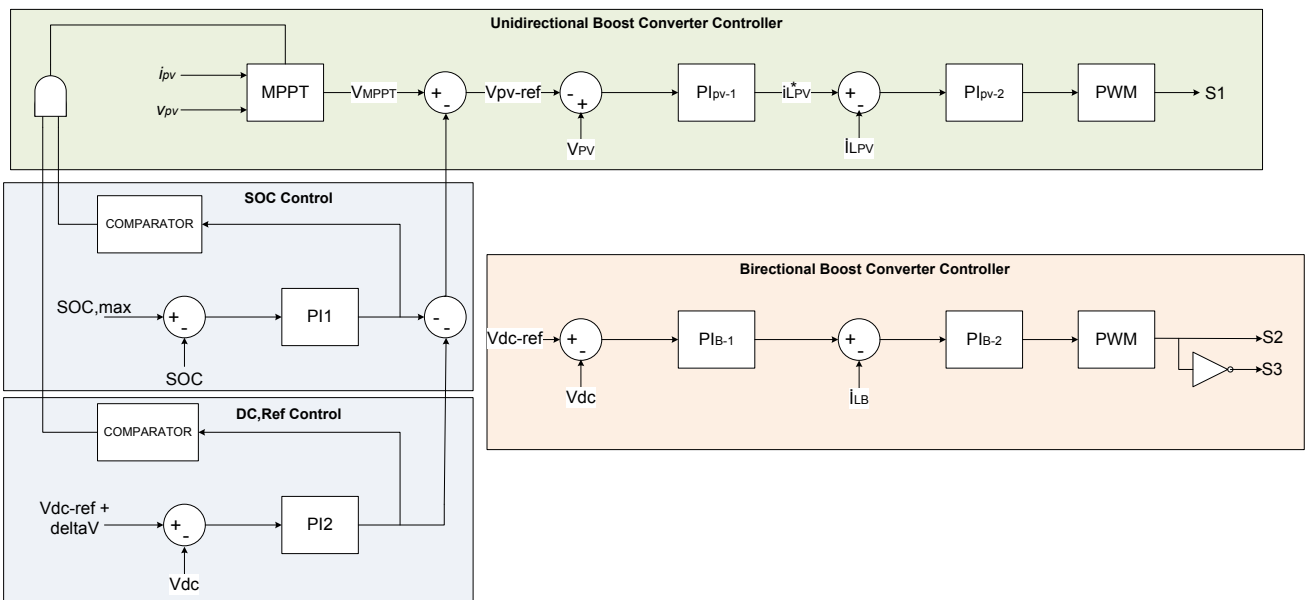


Fig. 2 – PV system control structure. [31].

$$G_{PI-pv_2} = 0.01 + 40 \frac{1}{s} \quad (6)$$

$$G_{PI-B_1} = 1 + 250 \frac{1}{s} \quad (7)$$

$$G_{PI-B_2} = 0.03 + 30 \frac{1}{s} \quad (8)$$

$$G_{PI-1} = 30.000 + 100.000 \frac{1}{s} \quad (9)$$

$$G_{PI-2} = 0.4 + 200 \frac{1}{s} \quad (10)$$

To operate PV panel at the maximum power point under various temperature and solar radiation levels, maximum power point tracking (MPPT) methods were utilized. For the MPPT, there are several methods described in the literature such as Perturb & Observe, Incremental Conductance, Current Sweep and Constant Voltage. Our first attempt implemented the Perturb & Observe (P&O) method because it is easy to program and produces satisfactory results when the PV panel power output is high enough. P&O algorithms make small changes in the PV panel terminal voltage during each control period and observe the change in the output power (ΔP). If $\Delta P > 0$, panel voltage is increased; if $\Delta P < 0$ panel voltage is decreased. In this manner the panel is driven to the maximum power point [32]. Unfortunately, after several tests, the P&O method was deemed to be inappropriate for our system because it has to work in winter at low irradiation levels and temperatures. These factors cause the panels to have low power output and a flatter P–V graph, which hinders the P&O algorithm's ability to find the maximum power point. Another drawback with P&O is that the PV system oscillates around the required operating point $\Delta P = 0$ because the panel voltage is perturbed during each MPPT control period. For these reasons the Incremental Conductance (IC) method was utilized in the final design. Under rapidly changing weather conditions, IC yielded better results as expected from past studies in literature [33]. Under the IC method, the slope (dP/dV) of the panel P–V graph is analyzed: dP/dV is zero at the maximum power point, negative to the right of the maximum power point, and positive to the left of the maximum power point.

Numerical realization in MATLAB/Simulink

The PV panel model for our study has to include variable irradiation and temperature inputs. As described in Refs. [34], taking into account the effects of temperature and irradiation on solar cell output current, PV array output current can be calculated as follows

$$I_{pv} = N_p I_{ph} - N_p I_s \left(e^{\frac{q(V+I_{pv}R_s)}{akT}} \right) - \frac{1}{R_p} \left(\frac{V}{N_s} + \frac{I_{pv}R_s}{N_p} \right) \quad (11)$$

where R_s is the series resistance of the cell model, R_p is the shunt resistance of the cell model, I_{ph} is the light generated current, I_s is the reverse saturation current of the diode, q is the electron charge, a is the diode ideality factor, T is the cell temperature in degrees Kelvin, N_s is the number of solar cells

connected in series and N_p is the number of solar panels connected in parallel in the array.

A PV array model that takes into account variable irradiation and temperature was developed according to Eq. (11) and developed in the Simulink environment, as shown in Fig. 3.

DC/DC converters are modeled as shown in Fig. 4 with MOSFET on resistances of 0.22 Ω , internal diode resistances 0.001 Ω , internal diode forward voltage 1.2 V and a snubber resistance 10 k Ω . The values for the other elements in the converters are $L_{pv} = 550 \mu\text{H}$, $C_{dc1} = 1200 \mu\text{F}$, $L_B = 880 \mu\text{H}$ and $C_{dc2} = 1200 \mu\text{F}$. A unidirectional boost converter is utilized for the MPPT operation and to step up the voltage from the PV panel to a constant 400 VDC. A bidirectional boost converter is utilized to charge and discharge the lead-acid battery and to step up the voltage from the 192 VDC battery voltage to the 400 VDC required during battery discharge.

A battery model based on [35–37] is utilized to model the lead acid battery and a control system with a nominal voltage of 192 V, rated capacity of 32 Ah and an initial 50% charge state, which is consistent with standard implementations in the literature [31]. To obtain the maximum power from the PV panel, an MPPT controller utilizing the IC algorithm is built using the Stateflow environment in MATLAB/Simulink, where the decision logic is easily implemented using state transitions within a flow chart.

The final model of the whole system ready for numerical simulation in MATLAB/Simulink is given in Fig. 5. The inside of the control system (orange (in the web version) block in the bottom right of Fig. 5) is shown in Fig. 6.

Controller redesign

Numerical simulation of the overall system is performed under the real environmental conditions for a sunny day and a cloudy day for Ankara, Turkey. Real irradiation data are obtained from the free online SoDa (Solar Radiation Data) database, and the real temperature values are obtained from the PVGIS (Photovoltaic Geographical Information System) database. The irradiation data resolution is 1 min, and the temperature data resolution is 15 min. Irradiation, temperature and load changes used during simulations are given in Figs. 7–9, respectively.

Since ambient temperature data given in Fig. 8 cannot be utilized directly as an input to the PV panel simulation given in Fig. 3, cell temperature estimation method given in Eq. (12) is utilized for such calculation [38].

$$T_{cell} = T_{amb} + \left(\frac{NOCT - 20}{80} \right) S \quad (12)$$

where T_{cell} is the PV panel's surface temperature ($^{\circ}\text{C}$), T_{amb} is the ambient temperature ($^{\circ}\text{C}$), NOCT is the nominal operating cell temperature of the PV panel ($^{\circ}\text{C}$) in an external environment of 80 mW/cm² irradiance, 20 $^{\circ}\text{C}$ ambient temperature and 1 m/s wind velocity and S is the ambient insolation (mW/cm²).

Typical values of NOCT range from about 48 $^{\circ}\text{C}$ to 60 $^{\circ}\text{C}$ depending the type of PV arrays, ground-mounted or roof-mounted [38]. NOCT for the ground-mounted Sanyo HIP-200BA3 200 W panel is 44.2 $^{\circ}\text{C}$ according to its datasheet.

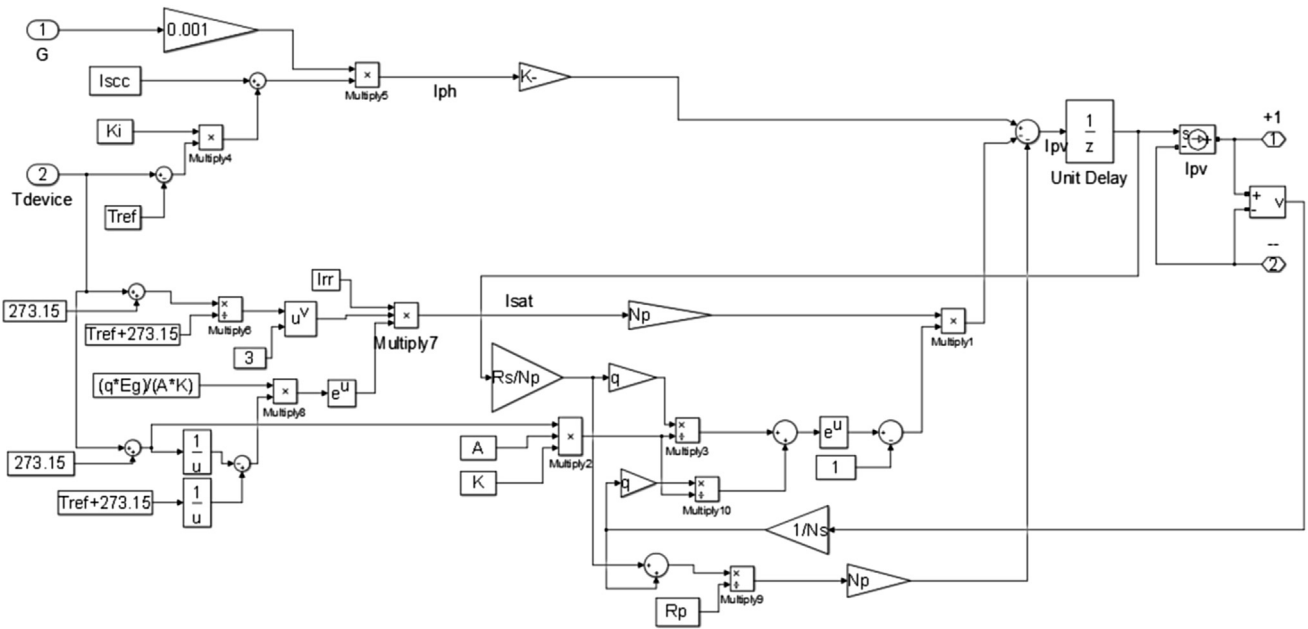


Fig. 3 – MATLAB/Simulink model of the PV array.

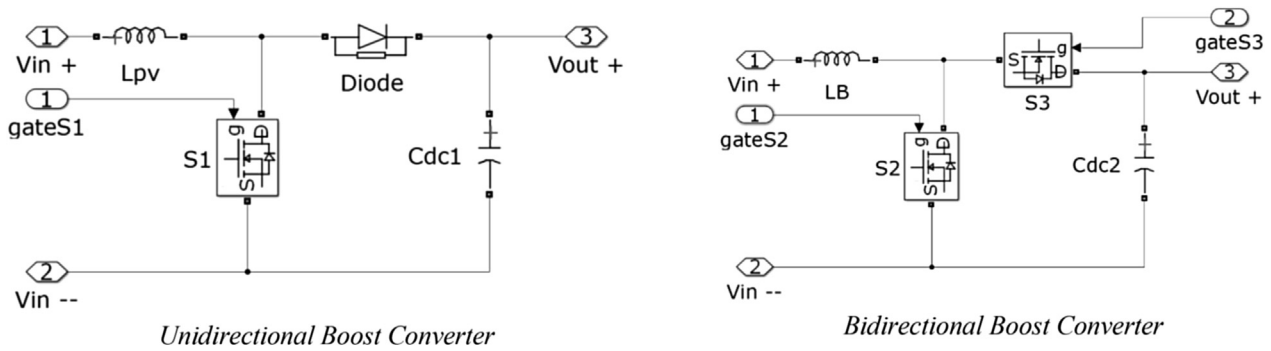


Fig. 4 – DC/DC converter models of the PV system.

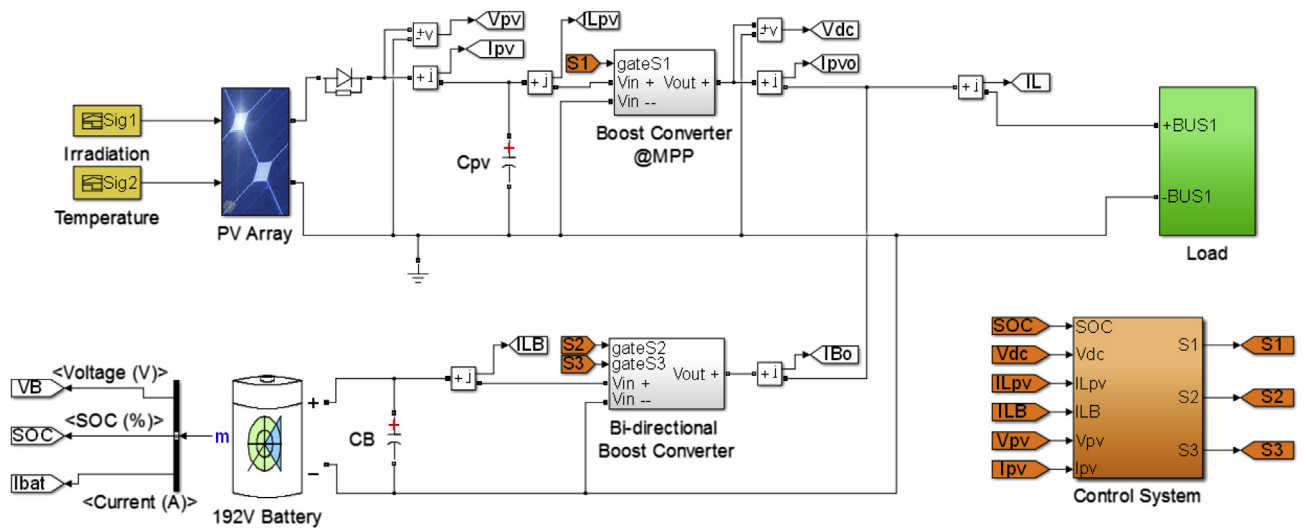


Fig. 5 – MATLAB/Simulink model of the whole PV system.

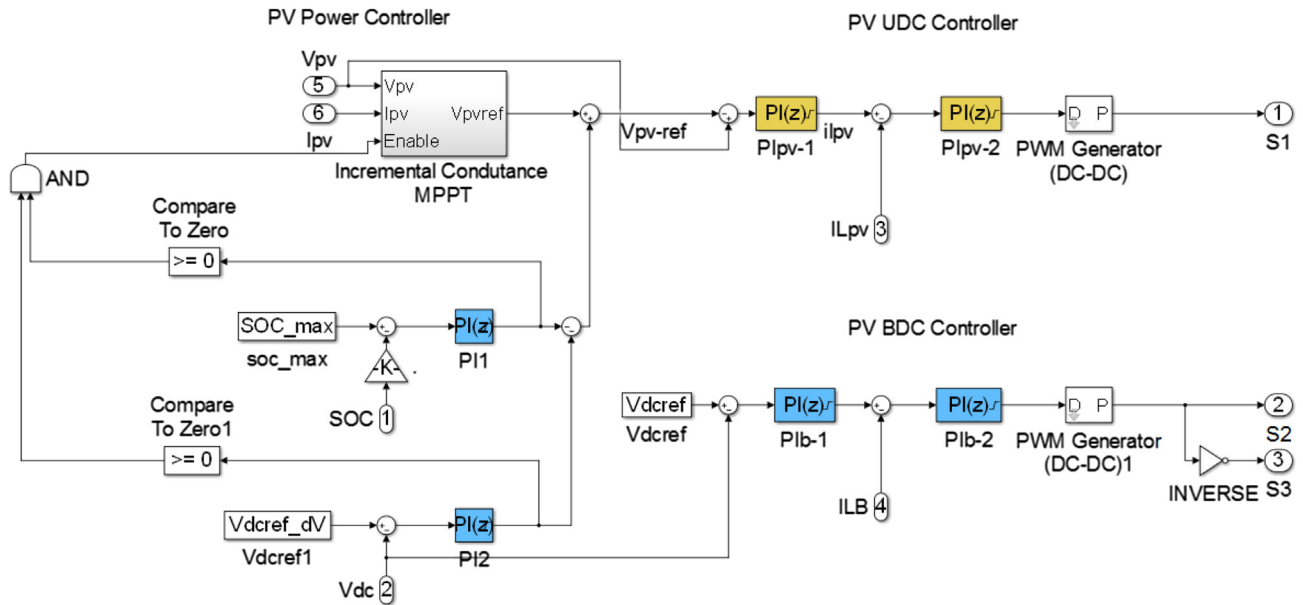


Fig. 6 – MATLAB/Simulink model of the control system.

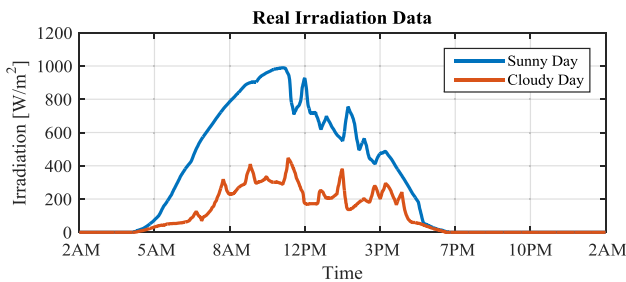


Fig. 7 – Ankara daily global irradiation data in sunny and cloudy weather.

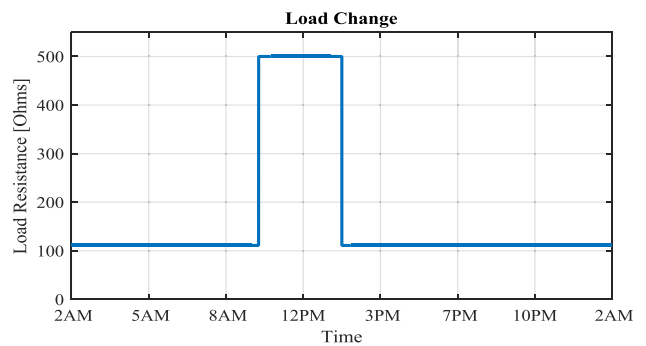


Fig. 9 – Load change from 500 Ω (maximum) to 111 Ω (minimum).

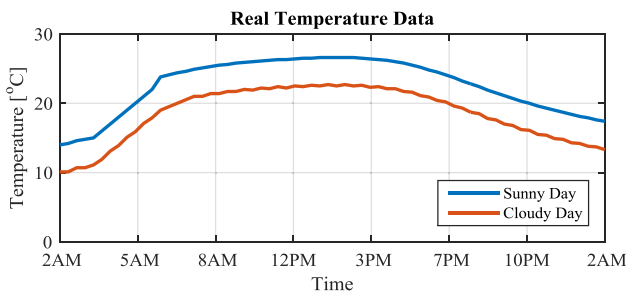


Fig. 8 – Ankara daily ambient temperature data in sunny and cloudy weather.

The PV system was simulated under sunny and cloudy weather conditions against the load change given in Fig. 9. The results obtained are given in Figs. 10 and 11. In cloudy weather conditions, the power from the sun was not enough to both supply sufficient current to the load and charge the battery. This does not affect the DC-link and the theoretically designed controllers (PI_{PV-1} and PI_{PV-2}) are able to provide constant DC voltage to the load, as shown in Fig. 11. However, in sunny weather conditions, there is enough power to both supply

sufficient current to the load and charge the battery with the excess power, and the DC-link is derogated. The theoretically designed PI controllers cannot adapt to the derogation, and there are 300 V_{p-p} voltage fluctuations on the load and 13 A_{p-p} current fluctuations of the battery charge current. These fluctuations can affect the critical load, health of the lead-acid and battery lifetime, which necessitated the redesign of the DC-link controllers.

There are many studies on PV system design in the literature based on the implementation of models, either numerically or experimentally, after which the controllers (usually PI controllers) are tuned empirically by trial-and-error to achieve acceptable performance [18–30]. However, this makes it difficult to judge the stability and robustness of the system so determining whether the controller will work under real conditions other than those under which it was designed is difficult. The main obstacle preventing a methodological design is the difficulty of obtaining simple analytical models on which the control design can take place. This is because the system contains switching behavior and large nonlinearities, which, unless a proper operating point is found, often result in

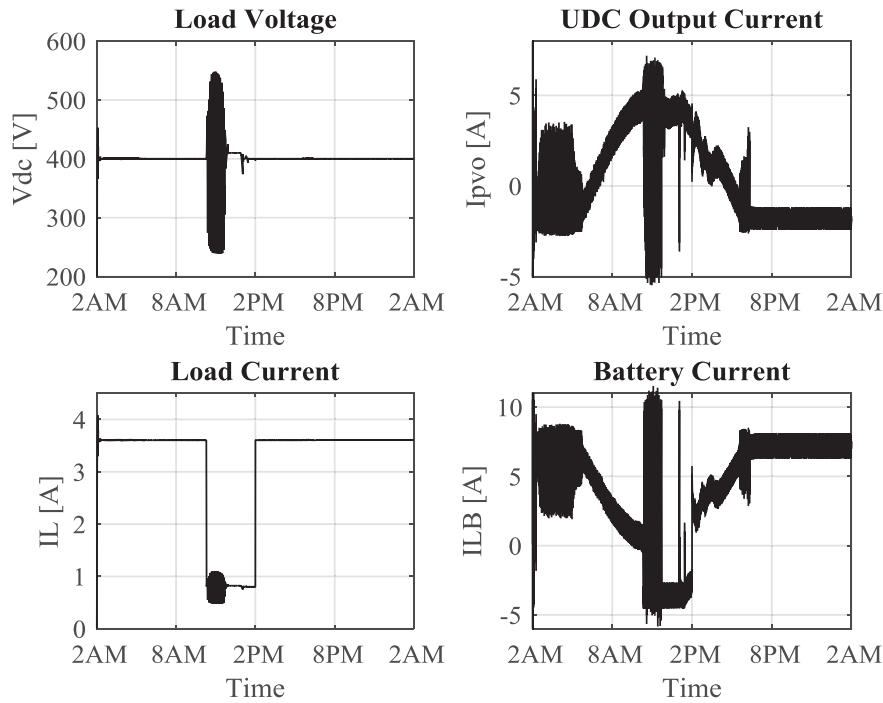


Fig. 10 – Standard system performance on a sunny day in Ankara.

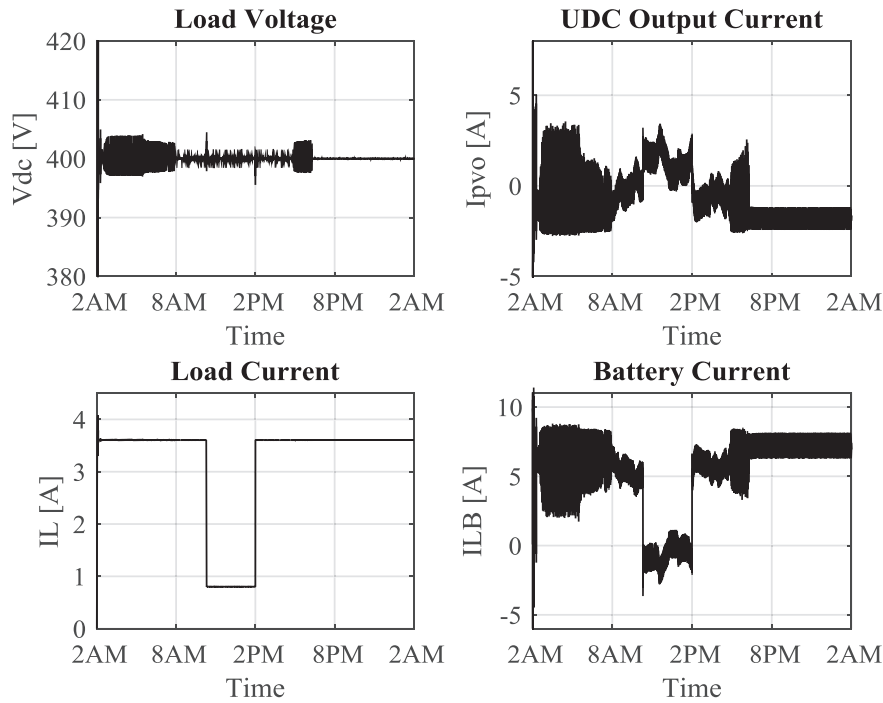


Fig. 11 – Standard system performance on a cloudy day in Ankara.

a nonlinearizable system. Without the use of advanced numerical tools to search for this point, this is not an easy task. This may explain why this direction has remained relatively unexplored in literature.

In our case, because there are two-level and three-level cascaded controllers as well as PWM driven switches in the system, it is difficult to theoretically find an accurate design for the controllers due to the nonlinear nature of the system.

In addition, each converter's controller dynamics are interdependent and these dynamics are changing with environmental conditions and critical load value. Therefore, it was important to design the controllers such that they could handle all known and unknown system dynamics.

A main difficulty in the systematic redesign of the PI_{B-1} and PI_{B-2} controllers responsible for DC-link control is that due to high-nonlinearities, standard linear modeling attempts fail

with the linearized system being identically zero. We therefore employed an alternative linearization approach based on bringing the system to a typical operating point using the system input and then providing a step change around this point. The data from this step change are used in the linearization procedure.¹

Identification data and the identified plant responses are shown in Fig. 12.

Among the various model formats available for data fit, the ones that seem to fit the best to the input/output system data

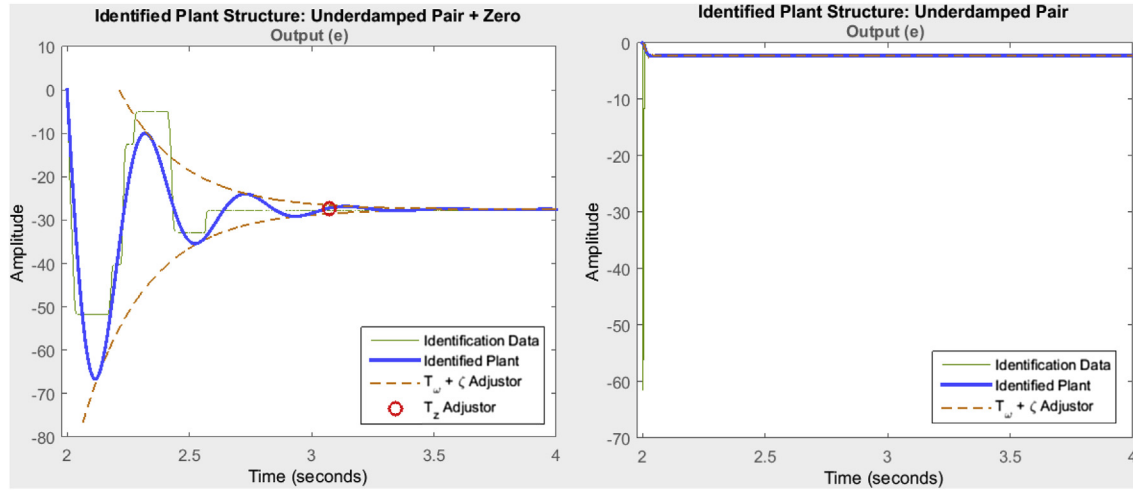


Fig. 12 – Identification data (green) and the identified plant response (blue) used in the controller design for the PI_{B-1} (left) and PI_{B-2} (right) subsystems. T_w , T_z and ζ Adjustors are related to the graphical fine tuning of the fit with an underdamped pair plant structure. (For interpretation of the references to colour in this figure legend, the reader is referred to the web version of this article.)

are the first and second order systems of the forms given in Eqs. (13) and (14).

$$G_{Plant_{B-1}} = \frac{27.526(1 + 0.142s)}{0.004s^2 + 0.0311s + 1} \quad (13)$$

$$G_{Plant_{B-2}} = \frac{44.657}{6.87 \times 10^{-5} s^2 + 0.0124s + 1} \quad (14)$$

These models denote two local linearized models around the operating point, as seen from the terminals of the respective controllers to be designed. Since we have obtained mathematical models of the system, we are no longer restricted to empirical PI controllers typical to many applications and we may investigate alternate strategies. As an example we build a Kalman-filter based optimal state controller, i.e. a Linear Quadratic-Gaussian (LQG) servo-controller [39,40]. Each of the plants in (13) and (14) can be expressed in an equivalent state-space representation as follows

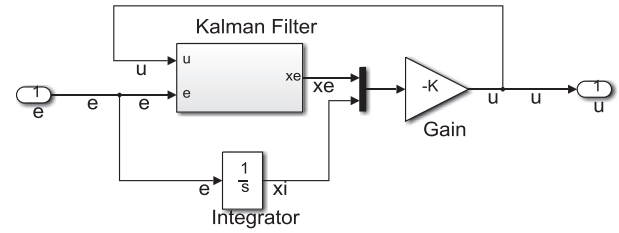


Fig. 13 – LQG controller with integral action and Kalman filter.

$$\begin{aligned} \frac{dx}{dt} &= Ax + Bu + w \\ y &= Cx + Du + v \end{aligned} \quad (15)$$

where x is the state vector, u is the plant input, y is the plant output, w is the process noise, v is the measurement noise and A , B , C , D are the state-space form matrices. LQG controller design minimizes the following cost function J

$$J = E \left\{ \lim_{\tau \rightarrow \infty} \frac{1}{\tau} \int_0^{\tau} x^T Q x + u^T R u + x_i^T Q_i x_i dt \right\} \quad (16)$$

where E denotes expected value, x_i is the integral of the reference tracking error of the output, and Q , R , Q_i are weighing for the states, inputs and integral error. An optimal value for a vector of gains denoted K is computed numerically to construct the control law $u = K[x \ x_i]^T$ so that J is minimized. Since the states x of the system are not directly measured, these are observed using a Kalman-filter, which produces an estimate x_e by minimizing

$$P = \lim_{t \rightarrow \infty} E \left\{ (x - x_e)(x - x_e)^T \right\} \quad (17)$$

using covariance matrices Q_n and R_n for the process and measurement noises respectively. This filter is known to

¹ In MATLAB/Simulink, this can be carried out by making the following selections from the menu: Plant → Identify New Plant → Plant Identification → Get I/O Data → Simulate Data → Simulate I/O Data.

provide solid estimates for the state vector even under noises and model/parametric uncertainties. The overall structure of the controller is given in Fig. 13.

The LQG controllers designed for plants (13) and (14) following the approach described above are

$$G_{LQG_{B-1}} = \frac{3641s^2 + 1.6 \times 10^5 s + 1.36 \times 10^6}{s^3 + 1.09 \times 10^4 s^2 + 2.87 \times 10^5 s} \quad (18)$$

$$G_{LQG_{B-2}} = \frac{5605s^2 + 8.73 \times 10^5 s + 5.43 \times 10^7}{s^3 + 2.59 \times 10^4 s^2 + 2.18 \times 10^7 s} \quad (19)$$

$$G(j\omega) = G_{\text{Plant}_{B-1}}(j\omega)G_{LQG_{B-1}}(j\omega) = \frac{-\omega^3 3.558 \times 10^6 j - 1.819 \times 10^8 \omega^2 + \omega 2.434 \times 10^9 j + 9.362 \times 10^9}{\omega^5 j + 10922.0 \omega^4 - \omega^3 3.723 \times 10^5 j - 4.962 \times 10^6 \omega^2 + \omega 7.181 \times 10^7 j}.$$

An additional point is that standard designs (e.g., [31]) include an upper limit on the DC-link voltage, e.g. it should not exceed 5% of V_{dc-ref} , but may not include a lower limit. This may be a handicap for the current objective of maintaining a constant DC-link voltage across a critical load. Therefore, the

the loop gain is allowed to increase without making the system unstable. The latter indicates how much phase lag can be tolerated in the loop before instability occurs. Parameter variations, uncertainties, noises and so on will perturb the nominal model, resulting in gain/phase variations so a robust system must be able to tolerate these to some extent. As a rule of thumb, control engineers aim for at least a 6 dB gain margin and 45° phase margin. The higher these are, the more perturbations the system can stand.

For the first loop we have

This can be written in standard complex number form

$$G(j\omega) = \text{Re}\{G(j\omega)\} + j\text{Im}\{G(j\omega)\}$$

where

$$\text{Re}\{G(j\omega)\} = -\frac{4.006 \times 10^{21} \omega^7 + 7.431 \times 10^{26} \omega^5 + 1.766 \times 10^{29} \omega^3 - 1.445e32 \omega}{1.126 \times 10^{15} \omega^9 + 1.335 \times 10^{23} \omega^7 + 3.424 \times 10^{25} \omega^5 - 3.249 \times 10^8 \omega^3 + 5.806 \times 10^{30} \omega}$$

control system design was modified to include both upper and lower limits for the DC-link voltage ($\pm 2.5\%$ of the V_{dc-ref}) as shown in Fig. 14. With this modification, DC-link regulation

and

$$\text{Im}\{G(j\omega)\} = -\frac{4.354 \times 10^{25} \omega^6 + 2.648 \times 10^{28} \omega^4 - 5.037 \times 10^{30} \omega^2 + 7.57 \times 10^{32}}{1.126 \times 10^{15} \omega^9 + 1.335 \times 10^{23} \omega^7 + 3.424 \times 10^{25} \omega^5 - 3.249 \times 10^{28} \omega^3 + 5.806 \times 10^{30} \omega}$$

control (PI₂ controller) does not have an effect when MPPT is enabled.

Results

In this section, we first determine the stability margins of the newly designed control loops using LQG method with integral action. Next, we perform a steady-state analysis for reference tracking. Then an investigation of the proposed architecture is performed under load changes when the PV panel and battery parameters contain uncertainties. Finally the system is tested with real environmental data under load changes.

Stability margins

There are many different indicators of a system's robustness. For sake of illustration we will compute the *gain margin* (GM) and *phase margin* (PM) [42]. The former measures of how much

The gain margin by definition is

$$GM = \frac{1}{|G(j\omega_{pc})|}$$

where ω_{pc} is the phase cross-over frequency, i.e. the frequency at which

$$\angle G(j\omega_{pc}) = 180^\circ.$$

The last equation requires that

$$\text{Im}\{G(j\omega)\} = 0.$$

It can be shown that the numerator of $\text{Im}\{G(j\omega)\}$ is never zero, that is

$$4.354 \times 10^{25} \omega^6 + 2.648 \times 10^{28} \omega^4 - 5.037 \times 10^{30} \omega^2 + 7.57 \times 10^{32} = 0$$

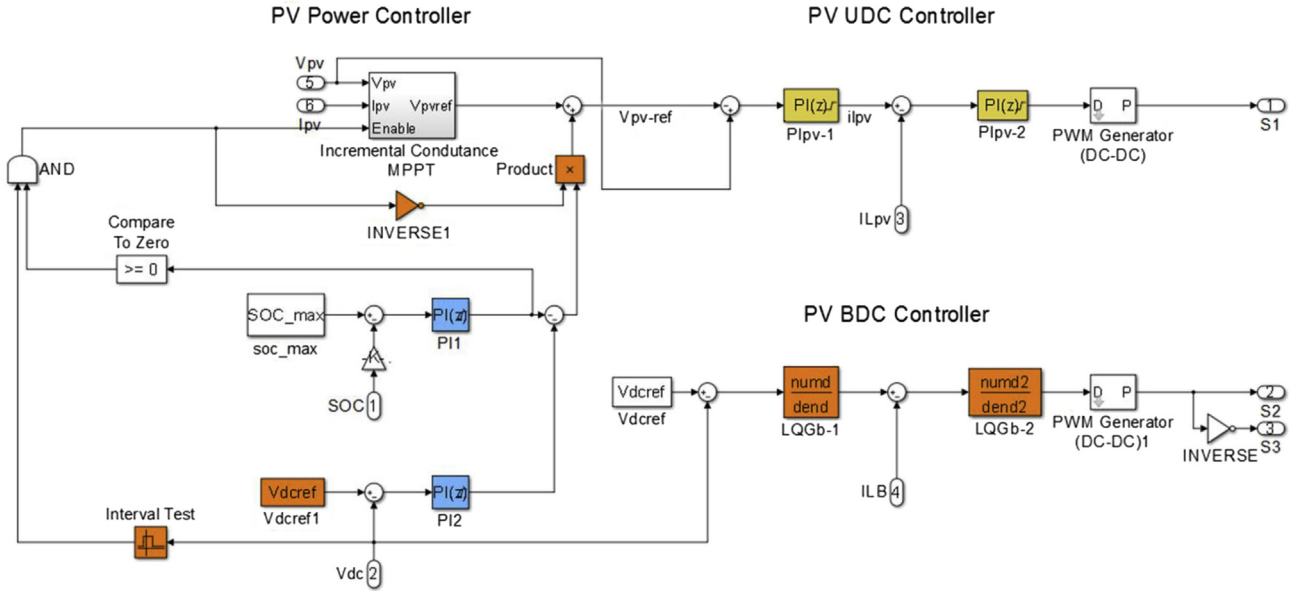


Fig. 14 – MATLAB/Simulink model of the modified control system.

has no real-valued solution for ω . This case is known as the ideal case since it means that the phase can never become 180° . It is referred to as *infinite gain margin* denoted as

$$GM = \infty.$$

The phase margin is defined as

$$PM = 180^\circ + \angle G(j\omega_{gc})$$

where ω_{gc} is the gain cross-over frequency at which

$$|G(j\omega_{gc})|^2 = 1.$$

we must therefore solve

$$|G(j\omega)|^2 = \frac{N(j\omega)}{D(j\omega)} = 1 \Leftrightarrow N(j\omega) = D(j\omega)$$

where $N(j\omega)$ and $D(j\omega)$ are the numerator and denominator of $|G(j\omega)|^2$ with values

$$N(j\omega) = 1.605 \times 10^{43} \omega^{14} + 1.902 \times 10^{51} \omega^{12} + 2.86 \times 10^{54} \omega^{10} + 5.239 \times 10^{56} \omega^8 - 3.844 \times 10^{59} \omega^6 + 1.44 \times 10^{61} \omega^4 + 1.326 \times 10^{64} \omega^2 + 5.73 \times 10^{65},$$

$$D(j\omega) = 1.268 \times 10^{30} \omega^{18} + 3.005 \times 10^{38} \omega^{16} + 1.781 \times 10^{46} \omega^{14} + 9.138 \times 10^{48} \omega^{12} - 7.5 \times 10^{51} \omega^{10} - 6.752 \times 10^{53} \omega^8 + 1.453 \times 10^{57} \omega^6 - 3.773 \times 10^{59} \omega^4 + 3.371 \times 10^{61} \omega^2.$$

Solving numerically for the positive real root yields

$$\omega_{gc} = 328.1386 \text{ rad/s.}$$

Evaluating

$$G(j\omega_{gc}) = -0.0816 - 0.9967j$$

which satisfies $G(j\omega_{gc}) = 1$ and its angle can be computed as

$$\angle G(j\omega_{gc}) = -94.6790^\circ.$$

Thus the phase margin is

$$PM = 180^\circ - 94.6790^\circ = 85.3210^\circ.$$

An identical computation can be carried out for the second loop with

$$G(j\omega) = G_{plant_{b-2}}(j\omega)G_{LQGb-2}(j\omega).$$

For sake of simplicity we omit the intermediate steps of the calculations, from where one obtains

$$\omega_{pc} = 4724.6 \text{ rad/s}$$

and

$$G(j\omega_{pc}) = -0.0062884.$$

Therefore

$$GM = \frac{1}{0.0062884} = 159.0219 = 44.0291 \text{ dB.}$$

For the phase margin one obtains

$$\omega_{gc} = 161.7419 \text{ rad/s}$$

and

$$G(j\omega_{gc}) = -0.0014139 - 0.9999j$$

which has $|G(j\omega_{gc})| = 1$ and

$$\angle G(j\omega_{gc}) = -90.081^\circ.$$

Thus the phase margin is

$$PM = 180^\circ - 90.081^\circ = 89.9190^\circ.$$

It is clear that both gain margins are well above 6 dB, and

phase margins are well above 45°, indicating very good robustness properties. This statement will be further confirmed with the uncertainty analysis in Section [Uncertainty Analysis](#).

Steady-state analysis

A steady-state analysis for reference tracking of the novel control loops designed using LQG design with integral action are computed in this section. Recall that the LQG control has integral action (see [Fig. 13](#)) to eliminate steady-state errors. Since neither the plants nor the controllers have any zeros at the origin, this makes the compensated system Type 1, meaning no steady state-error for step commands [42]. This is also confirmed by the following analysis. The transfer function from reference to error is

$$\frac{E(s)}{R(s)} = \frac{1}{1 + G(s)}$$

where $G(s)$ is the loop transfer function. For the first control loop we have

$$\begin{aligned} G(s) &= G_{\text{Plant}_{B-1}}(s)G_{\text{LQG}_{B-1}}(s) = \frac{27.526(1 + 0.142s)}{0.004s^2 + 0.0311s + 1} \times \frac{3641s^2 + 1.6 \times 10^5s + 1.36 \times 10^6}{s^3 + 1.09 \times 10^4s^2 + 2.87 \times 10^5s} \\ &= \frac{3.558 \times 10^6 s^3 + 1.819 \times 10^8 s^2 + 2.434 \times 10^9 s + 9.362 \times 10^9}{s^5 + 1.092 \times 10^4 s^4 + 3.723 \times 10^5 s^3 + 4.962 \times 10^6 s^2 + 7.181 \times 10^7 s} \end{aligned}$$

From final value theorem (FVT)

$$\begin{aligned} e_{ss} &= \lim_{t \rightarrow \infty} e(t) = \lim_{s \rightarrow 0} sE(s) = \lim_{s \rightarrow 0} \frac{s}{1 + G(s)} R(s) = \lim_{s \rightarrow 0} \frac{s}{1 + G(s)} \frac{1}{s} \\ &= \lim_{s \rightarrow 0} \frac{1}{1 + G(s)} = \frac{1}{\lim_{s \rightarrow 0} G(s)} = \frac{1}{K_p} \end{aligned}$$

where $K_p = \lim_{s \rightarrow 0} G(s)$ and we used the fact that $R(s) = \frac{1}{s}$ for a step command. Since clearly

$$K_v = \lim_{s \rightarrow 0} G(s) = \infty$$

this implies that

$$e_{ss} = 0.$$

The analysis can be carried out in an identical manner for the second control loop with

$$G(s) = G_{\text{Plant}_{B-2}}(s)G_{\text{LQG}_{B-2}}(s) = \frac{3.643 \times 10^9 s^2 + 5.679 \times 10^{11} s + 3.532 \times 10^{13}}{s^5 + 2.613 \times 10^4 s^4 + 2.638 \times 10^7 s^3 + 4.191 \times 10^9 s^2 + 3.178 \times 10^{11} s}$$

to once again obtain $e_{ss} = 0$. In summary there is no steady state error for both control loops.

For ramp-type inputs $R(s) = \frac{1}{s^2}$ so using FVT as above yields

$$\begin{aligned} e_{ss} &= \lim_{t \rightarrow \infty} e(t) = \lim_{s \rightarrow 0} sE(s) = \lim_{s \rightarrow 0} \frac{s}{1 + G(s)} R(s) = \lim_{s \rightarrow 0} \frac{s}{1 + G(s)} \frac{1}{s^2} \\ &= \lim_{s \rightarrow 0} \frac{1}{s + sG(s)} = \frac{1}{\lim_{s \rightarrow 0} sG(s)} = \frac{1}{K_v} \end{aligned}$$

For the first control loop

$$K_v = \lim_{s \rightarrow 0} sG(s) = 130.3767$$

so we have

$$e_{ss} = \frac{1}{K_v} = 0.0077$$

which is very small, indicating a good tracking of time-varying reference commands as well. For the second control loop

$$K_v = \lim_{s \rightarrow 0} sG(s) = 111.1421$$

so we have

$$e_{ss} = \frac{1}{K_v} = 0.0090$$

which is once again quite small.

Uncertainty analysis

The performance of a standard (i.e. PI) overall PV system [31] and that of the PV system outlined in this study (i.e. PI/LQG hybrid) are compared first at constant irradiation and temperature, and then using real weather data. To compare the system performance when the DC-link is interrupted, simulations were performed under constant irradiation (1000 W/m²) and ambient temperature (25 °C) values. Results are given in [Fig. 15](#).

According to [Fig. 15](#), the standard system becomes undamped when the load resistance is switched from the minimum to maximum at $t = 4$ s. The performance improves when the $\pm 2.5\%$ bound check is performed as described in the previous section. As a result, the 310 V_{p-p} oscillations for the high load case are eliminated. However, there are still oscillations of approximately 240 V_{p-p} during start-up and load

steps from the maximum to the minimum load, which is undesirable and can cause unpredicted damage for critical loads. The bidirectional converter's controllers are redesigned as described in the preceding section, and higher performance

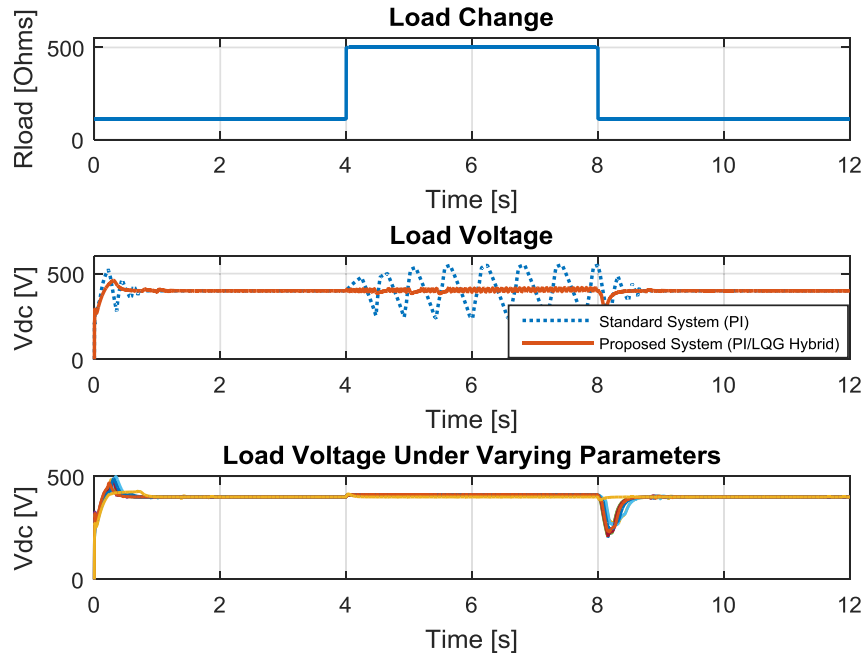


Fig. 15 – Performance comparison of standard and modified systems against load changes under constant irradiation (1000 W/m^2) and temperature (25°C) and uncertainty analysis of the modified system.

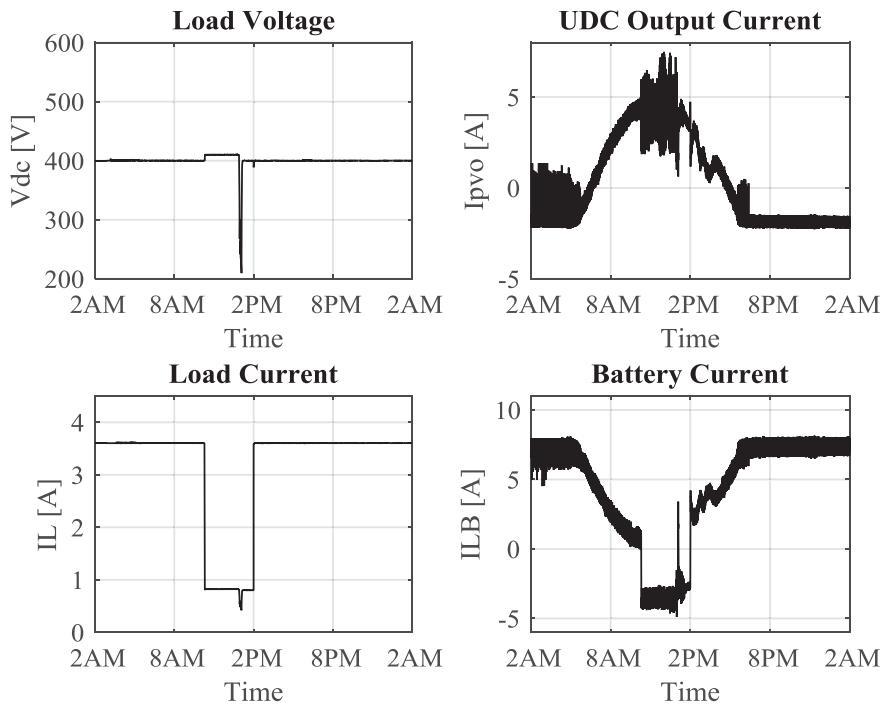


Fig. 16 – Modified system (with redesigned controllers) performance on a sunny day in Ankara.

is obtained both at start-up and during load steps from maximum load to minimum load and minimum load to maximum load as seen in Fig. 15.

Uncertainty analysis is also performed by randomly sampling the PV panel parameters (shunt resistance, series resistance, diode ideality factor and diode reverse saturation current, as shown in Eq. (11)) and lead-acid battery parameters

(battery capacity and nominal voltage, which changes all other parameters such as maximum capacity, nominal discharge current, internal resistance and exponential zones). In a real system those variables will likely be different than the ones used during the design and simulation. Ten random combinations of these parameters in the range of $\pm 20\%$ of their designed values were used in simulations to verify the

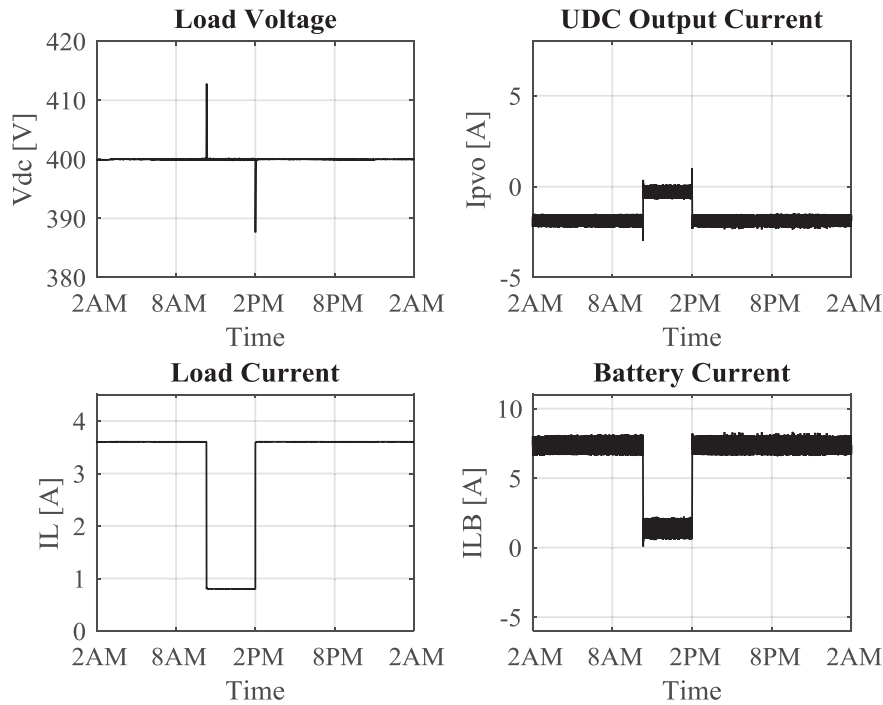


Fig. 17 – Modified system (with redesigned controllers) performance on a cloudy day in Ankara.

robustness of the control system. As shown in Fig. 15, the control system was robust enough to control the load voltage without being affected by those parameter variations.

Tests with real weather data

A modified system with redesigned controllers is simulated using real weather data for Ankara, as shown in Figs. 7 and 8,

and load changes, as shown in Fig. 9. The results obtained are shown in Figs. 16 and 17.

According to the standard design results given in Figs. 10 and 11, the battery current saturates at its maximum discharge value of 10 A and exhibits a peak change of 13.2 A between the charging and discharging states during a load change at high irradiation values. This is not healthy for the battery and can shorten its life cycle considerably. In addition there is a peak

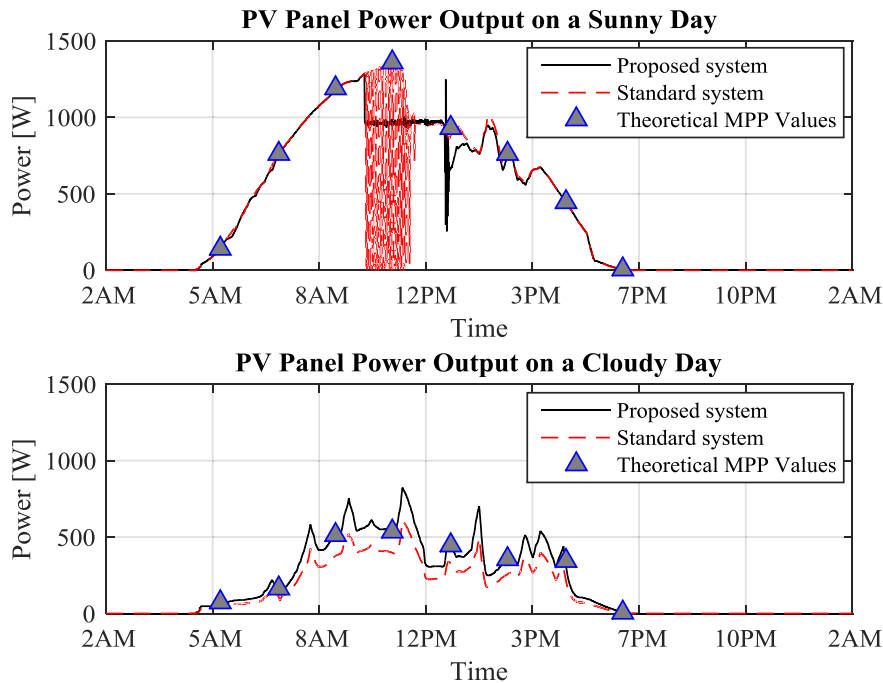


Fig. 18 – Maximum power point tracking performances of the PV System with standard control system and modified control system with redesigned controllers.

change of $300 V_{p-p}$ across the load, which can also cause damage. With the modification of the control system described in the previous section, it is therefore observed that the PV system designed following standard literature, with no methodological/modeling approach to each controller design, may have difficulty meeting the desired voltage and current limits on the load and the battery.

The modified control system performs much better given irradiation and temperature changes than the standard design in Ref. [31]. Its response during load variations slightly exceeds the allowed limits of $400 \pm 10VDC$. In the sunny day case, its response is within the allowed limits except when the load changes from the maximum of 500Ω to minimum of 111Ω at 2 PM and when the irradiation value dropped below a critical value. This causes the MPPT controller to start up again to provide power to the load and battery at 12.30 PM. There is a peak change of voltage across the load of approximately $190 V_{p-p}$ and a peak change of current through the battery of approximately $6.2 A_{p-p}$ which is not desirable. In the cloudy day case, its response is within the allowed limits except when the load was stepped from the minimum of 111Ω to the maximum 500Ω at about 10 AM, and from maximum to minimum at 2 PM. There is an undesired peak voltage change across the load of approximately $12 V_{p-p}$, and, as desired, there are no peak currents on the battery. Undesired voltage and current peaks on the load and battery are caused by the failure of single input single output (SISO) mode-based PI/LQG controllers to handle the highly nonlinear nature of multi input multi output (MIMO) PV systems caused by the use of PWM driven cascaded controllers.

It should also be noted that in addition to performing the tasks described in the paragraphs above, the controller is simultaneously attempting to keep the PV array at its maximum power point at all times. Maximum power points of the PV array composed of two parallel strings of four series-connected Sanyo HIP-200BA3 200 W panels and the maximum power point tracking performance of the Incremental Conductance method used in the PV system are shown in Fig. 18.

The proposed system contains redesigned novel controllers which perform better tracking of the references generated by the MPPT algorithm which results closer power values to theoretical MPPT values, which is especially visible for the cloudy day. For the sunny day, at many time instants more power is generated than required by the load and the battery charge limit combined. This results in the MPPT system being enabled and disabled several times during the scenario as compared to the cloudy day situation where it is always active. This has been identified as the reason for the poor performance of the standard system on the interval 9 AM – 11 AM for the sunny day. The only poor performance spot for the proposed system is at 12.30 PM. This is a point where the irradiation drops to a level so that the power is no longer enough for the load voltage regulation and battery charge simultaneously so the MPPT algorithm is reactivated. The transition causes a spike in the currents and voltages, which result in low performance for a short time duration. This is quickly recovered by the controller and good performance obtained again.

This demonstrates that the design always benefits as much from solar energy as possible and stores excess power in the battery with better response and efficiency than the standard control system.

Conclusions and future works

In this paper, a systematic modeling, simulation and controller design approach is outlined for a stand-alone photovoltaic (PV) system producing a constant DC output for critical loads. Obtaining simplified models for these systems and utilizing only theoretically designed model-based single input single output (SISO) controllers such as P/PI/PID are often problematic. This is because they contain elements such as switching DC/DC converters driven by pulse width modulation (PWM). This results in large nonlinearities that often produce nonlinearizable models when standard approaches are used. The methodology for the controller redesign presented in this paper is based on theoretical system modeling and the use of simulated input/output data to determine an operating point around which a linear system model is derivable according to the real model. After the model was obtained, linear quadratic Gaussian (LQG) servo-controller were designed for the bidirectional converter subsystems. In addition to the redesign of the controllers, an explicit check of the lower and upper bounds of the DC-link voltage was introduced based on which MPPT procedure can be disabled. This ensures that the system would abandon MPPT and focus entirely on providing the load with the correct voltage in case the voltage drifted to unacceptably high or low values. Through numerical simulations, it was confirmed that the modified control system resulted in a well damped response and improved robustness when compared to the PI-type controllers utilized in standard literature. The latter designs especially struggle to keep a steady output voltage when the load is increased. This is due to the inefficiency of the bidirectional converter controllers which are responsible for battery charge, battery discharge and DC-link voltage control, which must adapt to uncertainties, noises and variations of environmental conditions and load. This was confirmed by comparing the performance of standard controllers to the redesigned controllers developed in this paper during sudden load variations. The standard PI-only methods exhibited large load voltage oscillations, and switched multiple times between the charging and discharging states of the battery. Both of these events could potentially damage the load and decrease battery state-of-health (SOH). In contrast, the redesigned controllers based on mathematical models obtained from simulated input/output data displayed smaller fluctuations and a much smoother voltage and current response, possibly protecting the load and battery from severe damage and premature aging. In addition, the proposed controllers operated the PV panel at its maximum power point with high efficiency at all times, therefore fully utilizing the sunlight under varying atmospheric conditions and storing any excess power in the battery until battery charge current limit was reached.

Although the modified control system had better performance than a standard design, there are still some undesired voltage and current peaks on the load and battery. This is thought to be related to the multi-input multi-output (MIMO) nature of the system. This introduces coupling between the different channels, which is not explicitly addressed in a single-input single-output (SISO) design. Our future research plans include obtaining MIMO system models of the PV-system on which MIMO controller designs can be designed and tested. Control strategies such as sliding mode control (SMC), linear parameter varying (LPV) control, H_2/H_∞ robust control and model predictive control (MPC) will be considered to improve performance and robustness. We also plan to test the proposed method on alternative PV system configurations (e.g., [41,42]) and to build a physical setup for experimental verification.

Acknowledgments

The authors would like to thank Dr. Hisham Mahmood for his kind help and valuable discussions throughout the preparation of this article. We are also grateful to the TOBB ETU Libraries for providing electronic, printed and software resources that have rendered this study possible.

REFERENCES

- [1] Kadioğlu S, Tellioglu Z. Enerji kaynaklarının kullanımı ve çevreye etkileri. In: Proc. TMMOB Turkish Energy Symp. Novemb.12–14; 1996.
- [2] Deveci O, Onkol M, Unver HO, Ozturk Z. Design and development of a low-cost solar powered drip irrigation system using systems modeling language. J Clean Prod 2015;102:529–44. <http://dx.doi.org/10.1016/j.jclepro.2015.04.124>.
- [3] Suzuki M. Identifying roles of international institutions in clean energy technology innovation and diffusion in the developing countries: matching barriers with roles of the institutions. J Clean Prod 2014;98:229–40. <http://dx.doi.org/10.1016/j.jclepro.2014.08.070>.
- [4] Paredes-Sánchez JP, Villicaña-Ortiz E, Xiberta-Bernat J. Solar water pumping system for water mining environmental control in a slate mine of Spain. J Clean Prod 2015;87:501–4. <http://dx.doi.org/10.1016/j.jclepro.2014.10.047>.
- [5] Pacas JM, Molina MG, dos Santos EC. Design of a robust and efficient power electronic interface for the grid integration of solar photovoltaic generation systems. Int J Hydrogen Energy 2012;37:10076–82. <http://dx.doi.org/10.1016/j.ijhydene.2011.12.078>.
- [6] Molina MG, Espejo EJ. Modeling and simulation of grid-connected photovoltaic energy conversion systems. Int J Hydrogen Energy 2014;39:8702–7. <http://dx.doi.org/10.1016/j.ijhydene.2013.12.048>.
- [7] Linares L, Erickson RW, MacAlpine S, Brandemuehl M. Improved energy capture in series string photovoltaics via smart distributed power electronics. In: Conf Proc – IEEE Appl Power Electron Conf Expo – APEC; 2009. p. 904–10. <http://dx.doi.org/10.1109/APEC.2009.4802770>.
- [8] Selvaraj J, Rahim N a. Multilevel inverter for grid-connected PV system employing digital PI controller. IEEE Trans Ind Electron 2009;(56):149–58. <http://dx.doi.org/10.1109/TIE.2008.928116>.
- [9] Hussein KH. Maximum photovoltaic power tracking: an algorithm for rapidly changing atmospheric conditions. IEE Proc – Gener Transm Distrib 1995;142:59. <http://dx.doi.org/10.1049/ip-gtd:19951577>.
- [10] Layate Z, Bahi T, Abadlia I, Bouzeria H, Lekhchine S. Reactive power compensation control for three phase grid-connected photovoltaic generator. Int J Hydrogen Energy 2015;40:12619–26. <http://dx.doi.org/10.1016/j.ijhydene.2015.07.087>.
- [11] Patel H, Agarwal V. MPPT scheme for a PV-fed single-phase single-stage grid-connected inverter operating in CCM with only one current sensor. IEEE Trans Energy Convers 2009;(24):256–63. <http://dx.doi.org/10.1109/TEC.2008.2005282>.
- [12] Liu F, Duan S, Liu F, Liu B, Kang Y. A variable step size INC MPPT method for PV systems. IEEE Trans Ind Electron 2008;(55):2622–8. <http://dx.doi.org/10.1109/TIE.2008.920550>.
- [13] Petrone G, Spagnuolo G, Teodorescu R, Veerachary M, Vitelli M. Reliability issues in photovoltaic power processing systems. IEEE Trans Ind Electron 2008;(55):2569–80. <http://dx.doi.org/10.1109/TIE.2008.924016>.
- [14] Inthamoussou FA, De Battista H, Mantz RJ. New concept in maximum power tracking for the control of a photovoltaic/hydrogen system. Int J Hydrogen Energy 2012;37:14951–8. <http://dx.doi.org/10.1016/j.ijhydene.2012.01.176>.
- [15] Onat N. Recent developments in maximum power point tracking technologies for photovoltaic systems. Int J Photoenergy 2010;2010:1–11. <http://dx.doi.org/10.1155/2010/245316>.
- [16] Enrique JM, Durán E, Sidrach-de-Cardona M, Andújar JM. Theoretical assessment of the maximum power point tracking efficiency of photovoltaic facilities with different converter topologies. Sol Energy 2007;81:31–8. <http://dx.doi.org/10.1016/j.solener.2006.06.006>.
- [17] García P, Torreglosa JP, Fernández LM, Jurado F. Optimal energy management system for stand-alone wind turbine/photovoltaic/hydrogen/battery hybrid system with supervisory control based on fuzzy logic. Int J Hydrogen Energy 2013;38:14146–58. <http://dx.doi.org/10.1016/j.ijhydene.2013.08.106>.
- [18] Ke J, Xinbo R, Mengxiang Y, Min X. A hybrid fuel cell power system. IEEE Trans Ind Electron 2009;(56):1212–22. <http://dx.doi.org/10.1109/TIE.2008.2008336>.
- [19] Jiang Z, Dougal R a. A compact digitally controlled fuel cell/battery hybrid power source. IEEE Trans Ind Electron 2006;(53):1094–104. <http://dx.doi.org/10.1109/TIE.2006.878324>.
- [20] Maleki A, Askarzadeh A. Comparative study of artificial intelligence techniques for sizing of a hydrogen-based stand-alone photovoltaic/wind hybrid system. Int J Hydrogen Energy 2014;39:9973–84. <http://dx.doi.org/10.1016/j.ijhydene.2014.04.147>.
- [21] Wang C, Nehrir MH. Power management of a stand-alone wind/photovoltaic/fuel cell energy system. IEEE Trans Energy Convers 2008;(23):957–67. <http://dx.doi.org/10.1109/TEC.2007.914200>.
- [22] Khaligh A, Rahimi AM, Lee Y-J, Cao J, Emadi A, Andrews SD, et al. Digital control of an isolated active hybrid fuel cell/lithium battery power supply. IEEE Trans Veh Technol 2007;(56):3709–21. <http://dx.doi.org/10.1109/TVT.2007.901929>.
- [23] Kim SK, Jeon JH, Cho CH, Ahn JB, Kwon SH. Dynamic modeling and control of a grid-connected hybrid generation system with versatile power transfer. IEEE Trans Ind Electron 2008;(55):1677–88. <http://dx.doi.org/10.1109/TIE.2007.907662>.
- [24] Tofighi A, Kalantar M. Power management of PV/battery hybrid power source via passivity-based control. Renew

- Energy 2011;36:2440–50. <http://dx.doi.org/10.1016/j.renene.2011.01.029>.
- [25] Zhou K. Optimal energy management strategy and system sizing method for stand-alone photovoltaic-hydrogen systems. *Int J Hydrogen Energy* 2008;33:477–89. <http://dx.doi.org/10.1016/j.ijhydene.2007.09.027>.
- [26] Liao Z, Ruan X. A novel power management control strategy for stand-alone photovoltaic power system. In: 2009 IEEE 6th Int. Power Electron. Motion Control Conf., IEEE; 2009. p. 445–9. <http://dx.doi.org/10.1109/IPEMC.2009.5157429>.
- [27] Chiang SJ, Shieh HJ, Chen MC. Modeling and control of PV charger system with SEPIC converter. *IEEE Trans Ind Electron* 2009;(56):4344–53. <http://dx.doi.org/10.1109/TIE.2008.2005144>.
- [28] Deveci O, Kasnakoglu C. Control of a photovoltaic system operating at maximum power point and constant output voltage under different atmospheric conditions. *Int J Comp Electron Eng* 2015;7(4):240–7. <http://dx.doi.org/10.17706/IJCEE.2015.7.4.240-247>.
- [29] Parsekar S, Chatterjee K. A novel strategy for battery placement in standalone solar photovoltaic converter system. In: 2014 IEEE 40th Photovolt. Spec. Conf., IEEE; 2014. p. 2751–6. <http://dx.doi.org/10.1109/PVSC.2014.6925498>.
- [30] Prodromidis GN, Coutelieris FA. Simulation and optimization of a stand-alone power plant based on renewable energy sources. *Int J Hydrogen Energy* 2010;35:10599–603. <http://dx.doi.org/10.1016/j.ijhydene.2010.07.065>.
- [31] Mahmood H, Michaelson D, Jiang J. Control strategy for a standalone PV/battery hybrid system. In: IECON 2012-38th Annu. Conf. IEEE Ind. Electron. Soc., IEEE; 2012. p. 3412–8. <http://dx.doi.org/10.1109/IECON.2012.6389351>.
- [32] Yafaoui A, Wu B, Cheung R. Implementation of maximum power point tracking algorithm for residential photovoltaic systems. *2nd Can Sol Build Conf* 2007:1–6.
- [33] De Brito M a G, Sampaio LP, Luigi G, E Melo G a, Canesin C a. Comparative analysis of MPPT techniques for PV applications. In: 3rd Int Conf Clean Electr Power Renew Energy Resour Impact, ICCEP 2011; 2011. p. 99–104. <http://dx.doi.org/10.1109/ICCEP.2011.6036361>.
- [34] Kim IS, Kim MB, Youn MJ. New maximum power point tracker using sliding-mode observer for estimation of solar array current in the grid-connected photovoltaic system. *IEEE Trans Ind Electron* 2006;(53):1027–35. <http://dx.doi.org/10.1109/TIE.2006.878331>.
- [35] Tremblay O, Dessaint L a. Experimental validation of a battery dynamic model for EV applications. *World Electr Veh J* 2009;3:1–10.
- [36] Zhu C, Li X, Song L, Xiang L. Development of a theoretically based thermal model for lithium ion battery pack. *J Power Sources* 2013;223:155–64. <http://dx.doi.org/10.1016/j.jpowsour.2012.09.035>.
- [37] Saw LH, Somasundaram K, Ye Y, Tay O. Electro-thermal analysis of lithium iron phosphate battery for electric vehicles. *J Power Sources* 2014;249:231–8. <http://dx.doi.org/10.1016/j.jpowsour.2013.10.052>.
- [38] Ioannou AK, Stefanakis NE, Boudouvis AG. Design optimization of residential grid-connected photovoltaics on rooftops. *Energy Build* 2014;76:588–96. <http://dx.doi.org/10.1016/j.enbuild.2014.03.019>.
- [39] Green M, Limebeer DJN. *Linear robust control*. Dover Publications; 2012.
- [40] Lopez CP. *MATLAB control systems engineering*. Apress; 2014.
- [41] Morani M. Robust process control. *Chem Eng Res Des* 1987;65:462–79. [http://dx.doi.org/10.1016/0009-2509\(90\)85041-B](http://dx.doi.org/10.1016/0009-2509(90)85041-B).
- [42] Kluever CA. *Dynamic systems: modeling, simulation, and control*. John Wiley & Sons; 2015.